ACS APPLIED MATERIALS & INTERFACES

www.acsami.org

Research Article

All-Inkjet-Printed Flexible Nanobio-Devices with Efficient Electrochemical Coupling Using Amphiphilic Biomaterials

Tae-Hyung Kang, Seung-Woo Lee, Kyowook Hwang, Wonbo Shim, Ki-Young Lee, Jung-Ah Lim, Woong-Ryeol Yu,* In-Suk Choi,* and Hyunjung Yi*

Cite This: *ACS Appl. Mater. Interfaces* 2020, 12, 24231−24241

Read Online

ACCESS | Metrics & More | Article Recommendations | Supporting Information

ABSTRACT: Nanostructured flexible electrodes with biological compatibility and intimate electrochemical coupling provide attractive solutions for various emerging bioelectronics and biosensor applications. Here, we develop all-inkjet-printed flexible nanobio-devices with excellent electrochemical coupling by employing amphiphilic biomaterial, an M13 phage, numerical simulation of single-drop formulation, and rational formulations of nanobio-ink. Inkjet-printed nanonetwork-structured electrodes of single-walled carbon nanotubes and M13 phage show efficient electrochemical coupling and hydrostability. Additive printing of the nanobio-inks also allows for systematic control of the physical and chemical properties of patterned electrodes and devices. All-inkjet-printed electrochemical field-effect transistors successfully exhibit pH-sensitive electrical current modulation. Moreover, all-inkjet-printed electrochemical biosensors fabricated via sequential inkjet-printing of the nanobio-ink, electrolytes, and enzyme solutions enable direct electrical coupling within the printed electrodes and detect glucose concentrations at as low as 20 μM. Glucose levels in sweat are successfully measured, and the change in sweat glucose levels is shown to be highly correlated with blood glucose levels. Synergistic combination of additive fabrication by inkjet-printing with directed assembly of nanostructured electrodes by functional biomaterials could provide an efficient means of developing bioelectronic devices for personalized medicine, digital healthcare, and emerging biomimetic devices.

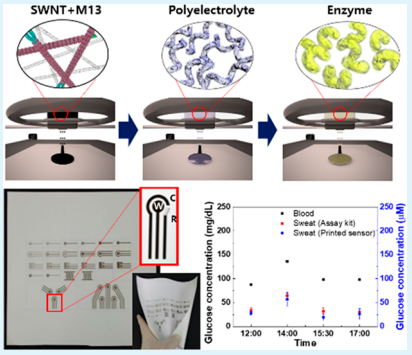

KEYWORDS: *inkjet-printing, amphiphilic biomaterials, single-walled carbon nanotubes, glucose biosensors, bioelectronics*

INTRODUCTION

Intimate electrochemical coupling between biological materials and electronic materials has been of tremendous importance for various bioelectronic devices and electrochemical biosensors for digital healthcare, point-of-care, and biomimetic devices.[1−4] Nanostructured electrodes have been widely explored for intimate electrical contact with biological materials owing to their comparable dimensions with biological materials and large effective surface area.[3,5] Various fabrication processes using nanomaterials have been developed for excellent electrochemical coupling between biological and electronic materials.[6,7] Specifically, solution-based processes of nanomaterials, such as drop-casting, screen printing, and inkjet printing are attractive because those processes are compatible with biological materials.[8,9] Among these, an inkjet printing method which deposits digitally controlled ejected drops of inks on specific locations of the substrate in a noncontact manner is particularly useful for device fabrication owing to the greater control of the spatial resolution of the printed electrodes, broad range of printable materials, high reproducibility, and additive and direct patterning capability.[10] However, to inkjet print nanobio-hybrid electrodes, inks must be carefully formulated for ensuring both stable jetting and hydrostability of printed electrodes.

For stable jetting, nano inks should possess colloidal stability and satisfy specific rheological conditions. In general, most pristine electronic materials, including nanocarbon materials such as carbon nanotubes, carbon nanofiber, and graphene, are hydrophobic and are prone to aggregation in aqueous solution unless appropriate functionalization is carried out. Chemical functionalization of nanomaterials enhances the colloidal stability, but it can degrade the intrinsic electronic properties of nanomaterials and can suffer from dissolution of printed electrodes in an aqueous environment. Uniform dispersion of nanomaterials via physical means, e.g., using small surfactant molecules or polymers, can retain their excellent electronic properties. However, the dissolution of printed electrodes made of surfactant-dispersed nanomaterials during washing and the prohibited intimate electrochemical coupling by polymer coating are major issues of physical functionalization. Also, the printing condition should be mild enough to retain

Received: February 11, 2020
Accepted: April 30, 2020
Published: April 30, 2020

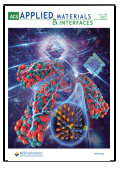

https://dx.doi.org/10.1021/acsami.0c02596
ACS Appl. Mater. Interfaces 2020, 12, 24231−24241

the functionality of biological materials, including enzymes. Therefore, the formulation of inks that enable colloidal stability and hydrostability and intimate electrical coupling of nanostructured electrodes and their inkjet printing technology should be studied strategically.

Peptides can bind electronic materials via molecular recognition and provide additional functionalities to the electronic material without chemical functionalizations.[11−16] An M13 phage, a filamentous biological material that expresses peptides on its body surface for strong binding with graphene and single-walled carbon nanotubes (SWNTs) has been successfully demonstrated to assemble nanocarbon materials onto functional electrodes with highly controlled nanostructures and material properties.[3,14,16−18] In particular, the hydrophobic segments of the amphiphilic body surface proteins of the M13 phage enabled stable binding with SWNTs through their long length in aqueous conditions, while the remaining hydrophilic segments provided additional functionality to the SWNTs in a nondestructive manner.[3,18] However, few studies have been performed for the inkjet printing of such nanobio complexes, although such an approach would greatly facilitate the fabrication of bioelectronic devices and sensors with high-performance.

Herein, we developed all-inkjet-printed flexible nanobio-devices with excellent electrochemical coupling capabilities by employing amphiphilic biological material, M13 phage, numerical simulation of single-drop formulation, and rational formulations of nanobio-ink. The numerical simulation of jetting behavior enabled the single-drop formation of the nanobio-ink. Moreover, the use of biological template materials in combination with inkjet printing technology allowed for the directed assembly of nanostructured hybrid electrodes with controllable physical and chemical properties in a scalable manner. All-inkjet-printed electrochemical field-effect transistors exhibited pH-sensitive electrical current modulations. In addition, the all-inkjet-printed enzymatic biosensors successfully detected the glucose levels in human sweat and showed a correlation with blood glucose levels. The current work presents a potentially powerful approach for fabricating high-performance nanobio-devices for digital healthcare, point-of-care, and emerging bioelectronic devices.

EXPERIMENTAL SECTION

Preparation of Nanobio-Ink Solutions. The as-received SWNT solution (1000 μg mL^{-1}, SuperPure SWNTs, Nanointegris Inc.) was surfactant-exchanged with sodium cholate (SC) solution (2% w/v in deionized water) using dialysis method (dialysis membrane product #132706, MWCO 12 000−14 000 Da, SpectraLabs). M13 phage clones expressing specific peptide sequences on its body surface for strong binding affinity toward SWNTs were prepared according to a previously reported method.[18] Briefly, the M13 phage clone was amplified using *E. coli* (XL-1 Blue, Stratagene) in a shaking incubator and centrifuged. The amplified M13 phage that remained in the supernatant was purified using the polyethylene glycol (PEG)/NaCl precipitation method and dissolved in Tris-buffered saline (TBS) solution. Polyethylenimine (PEI) (Mn 60 000 g mol^{-1}, Sigma-Aldrich) was dissolved in deionized (DI) water, and glucose oxidase (GOx) enzyme solutions were prepared in 10 mM phosphate-buffered saline (PBS) solution.

Numerical Simulation and Optimization of Inkjet Printing Conditions. The numerical simulation was performed to determine the processing parameters under which the solution formed a single drop. Comsol Multiphysics was used to simulate the jetting behavior of the SWNT−M13 nanobio-ink (10:1). The simulations were based on a structured Eulerian grid, a finite element discretization, and a level-set method. Simulation details are described in the Supporting Information (SI). A piezoelectric-type inkjet printer equipped with 16 nozzle-cartridge (DMC-11610, Fujifilm) was used. Drops were generated by shear mode actuators based on the reverse piezoelectric effect, and the droplet jetting was concomitantly monitored by a stroboscopic method using LED light for synchronization. The images of moving drops from the nozzle were taken at 5−10 μs interval up to 100 μs.

Fabrication of All-Inkjet-Printed Electrochemical Field-Effect-Transistors. For the source (S), drain (D), and gate (G) electrodes, 10 layers of a molar ratio of SWNT/M13 phage = 10:1 were inkjet-printed. The size of the S and D electrodes was 2 mm (H) × 1 mm (W), and the S and D electrodes were separated by 300 μm. To form a semiconducting channel, a single layer of a nanobio-ink of a molar ratio of SWNT/M13 phage = 2:2, which had a lower SWNT concentration and a higher M13 phage concentration, was inkjet-printed between the S and D electrodes.

Fabrication of All-Inkjet-Printed Electrochemical Glucose Biosensors. SWNT−M13 nanobio-ink of a molar ratio of SWNT/M13 phage = 10:1 was inkjet-printed on a glossy paper (Hansol, glossy photo paper). The printed electrodes were rinsed using DI water to remove residual surfactants and TBS and dried in ambient conditions. In order to nondestructively and intimately couple negatively charged GOx enzymes (isoelectric point (IEP) ≈ 4.3), a positively charged polyelectrolyte (PEI) solution was first inkjet-printed on the negatively charged SWNT−M13 nanobio-electrode and dried. Then, excess polyelectrolyte was rinsed using DI water and dried. Ten layers of enzyme ink solution were inkjet-printed on the PEI-coated SWNT−M13 electrodes. To construct the reference electrode, a commercial Ag/AgCl paste (ALS. Co., Ltd.) was screen printed to the inkjet-printed electrode using a prepatterned stencil mask. After applying the paste, the electrode was dried at room temperature for 1 h to evaporate the remaining solvent in the paste, and then washed with DI water and dried.

Characterization. The sheet resistance of the inkjet-printed nanobio-electrodes was measured using the van der Pauw method (HMS-3000, Ecopia). The thickness was measured using a surface profiler (KLA-Tencor Alpha-Step IQ, KLA-Tencor). The surface morphologies of the printed electrodes were examined using scanning electron microscopy (SEM) (Nova Nano SEM 200 (FEI) and JSM-7600F (JEOL)). For transmission electron microscopy (TEM), the nanobio-ink of SWNTs and M13 phage was printed on a TEM grid (Ted Pella, Carbon Grid Type-A, 300 mesh, Cu), washed with DI water, and then dried at room temperature. TEM analysis was performed using FEI Titan operated at 80−200 kV. Energy-filtered transmission electron microscopy (EF-TEM) was done using a Quantum 966 of FEI Titan, operated at 300 kV. All the electrochemical measurements were performed using a PARSTAT MC potentiostat (Princeton Applied Research). The transfer characteristics and output curves of the eFET were measured after dropping 10 μL of 10 mM phosphate-citrate buffer into an open region of a water-proof tape (3M #851 PCB PET SILICON ADHESIVE TAPE). For the flexibility test, the all-inkjet-printed enzymatic biosensors were completely folded and unfolded, and the change in the reduction peak current was measured after every four times folding up to 16 times. Cyclic voltammetry (CV) measurements were performed at a scan rate of 200 mV s^{-1} unless otherwise indicated.

Analysis of Sweat and Blood Glucose Levels. The study was performed based on the regulation of the institutional review board (IRB) of the Korea Institute of Science and Technology (KIST, IRB#: 2016−024). Two healthy males without a history of heart disease or diabetes participated in this study as volunteers. All subjects were informed of and agreed to the risks and benefits. Biological fluids were collected four times at intervals of every 90−120 min. Blood glucose level was measured using a commercial blood glucose meter (CareSens N Premier, i-SENS, Inc.). Approximately one μL of blood from the fingertip was collected for analysis. The sweat was collected using a cotton pad (Salivett, Sarstedt, Numbrecht, Germany) attached to the bodies of the volunteers by centrifugation.

https://dx.doi.org/10.1021/acsami.0c02596
ACS Appl. Mater. Interfaces 2020, 12, 24231−24241

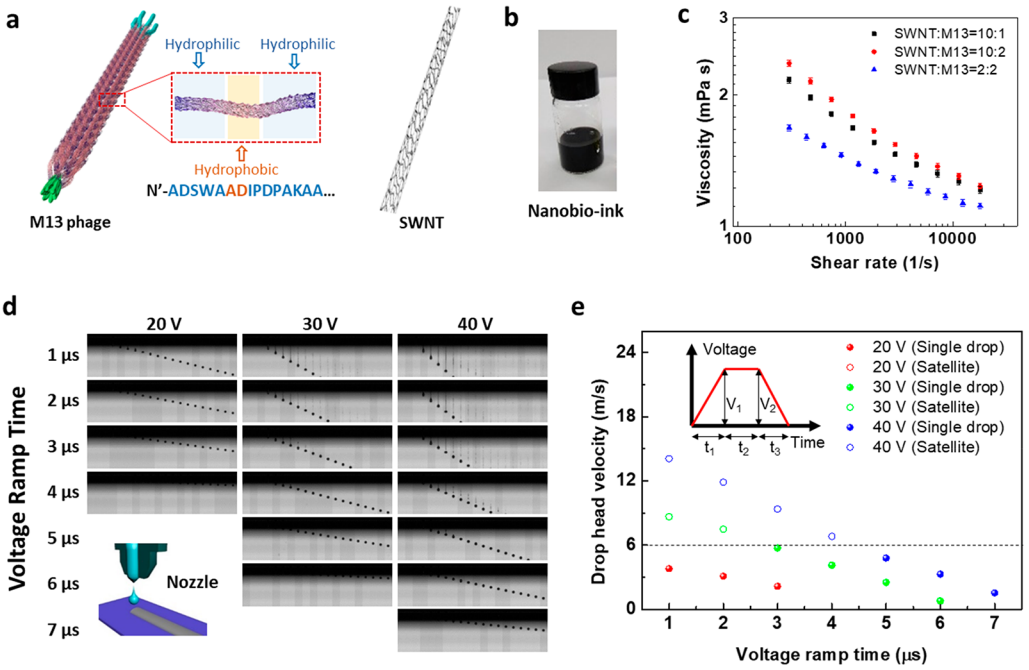

Figure 1. (a) Main components of the nanobio-ink: (i) biological material, M13 phage displaying amphiphilic peptide sequences on its body surface for strong binding to single-walled carbon nanotubes (SWNTs) and (ii) SWNTs to serve as nanoscale electronic materials. SWNTs were dispersed in aqueous solution using sodium cholate (SC) surfactants. The amino acid sequences corresponding to the hydrophobic and hydrophilic segments are colored as orange and blue, respectively. (b) Photograph of the nanobio-ink solution. (c) Dynamic viscosity of the SWNT−M13 phage solution in 1.3% sodium cholate and 13 mM TBS solution at 25 °C. (d) A series of snapshots of the ejected conductive nanobio-inks jetted at various voltages (V_1) and ramp times (t_1). A molar ratio of SWNT/M13 phage = 10:1 was used for the ink. The snapshots were taken for 100 μs at an interval of 5 μs. Inset: Illustration of jetting of the nanobio-ink onto the substrate through a piezoelectrically controlled nozzle. (e) Drop head velocity at various applied voltage values ($V = V_1 = V_2$) and voltage ramp time (t_1). The t_2 and t_3 were fixed as 5 and 10 μs. The results suggested that a single drop was formed when the head velocity of the nanobio-ink was 1.5−5.7 m s^{-1}.

Table 1. Physical Properties of Various Inks Formulated for the All-Inkjet-Printed Enzymatic Glucose Sensor[a]

ink	base solution	concentration	viscosity (mPa s)	surface tension (mN m^{-1})	Z
SWNT−M13 solution[b,d]	SC 1.3% w/v TBS 13 mM aqueous solution	SWNT: 2 × 10^{13} #/mL M13: 2 × 10^{12} #/mL	1.21 ± 0.022	50 ± 4	26.1
		SWNT: 2 × 10^{13} #/mL M13: 4 × 10^{12} #/mL	1.23 ± 0.017	48 ± 6	25.2
		SWNT: 4 × 10^{12} #/mL M13: 4 × 10^{12} #/mL	1.11 ± 0.017	49 ± 5	28.2
PEI solution[c,e]	DI water	5% w/v	4.03 ± 0.031	71.2 ± 0.2	9.4
GOx solution[c,e]	PBS 10 mM aqueous solution	25 mg/mL	1.22 ± 0.019	62.3 ± 0.1	28.9

[a]Three and five samples were used for the calculation of mean values ± SD of the viscosity and surface tension, respectively. $Z = (a\rho\gamma)^{1/2}/\eta$ where ρ, γ, η, and a are density, surface tension, viscosity, and characteristic dimension length, respectively. [b]Measured at shear rate = 20 000 s^{-1}. [c]Measured at shear rate = 100 s^{-1} [d]Measured by pendant drop method. [e]Measured by Du nouy ring method

The collected sweat was characterized using both the newly developed all-inkjet-printed glucose biosensor and the commercial glucose assay kit (Product Number: GAGO-20, Sigma-Aldrich) and their results were then compared.

RESULTS AND DISCUSSION

The main components of the nanobio-ink, that is, an M13 phage clone displaying peptide sequences on its body coat proteins for strong binding affinity toward SWNTs and the SWNTs are schematically illustrated in Figure 1a.[18,19] The specific body coat proteins of the M13 phage are amphiphilic,[18,20] wherein a hydrophobic segment is sandwiched by hydrophilic segments, as depicted in Figure 1a. The hydrophobicity plot was calculated based on the Kyte-Doolittle scale.[18,21] The amino acid sequences corresponding to the hydrophobic and hydrophilic segments are colored as orange and blue, respectively. The hydrophobic segment of the body coat proteins preferentially interacts with the hydrophobic sidewall of SWNTs along the length of the M13 phage,[18] and the hydrophilic segment stabilizes the M13 phage−SWNT complex in the aqueous solution once the complexes are formed. To prepare the nanobio-ink, each SWNT and M13 phage solution was mixed to achieve a final molar ratio of SWNT/M13 phage = 10:1, 10:2, or 2:2 in a total volume of 2 mL of 1.3% w/v sodium cholate and 13 mM TBS solution. Note that other additives were not used in this study because remaining additives after washing could hinder intimate electrical coupling within printed nanobio-electrodes. A photograph of the nanobio-ink solution is shown in Figure 1b. The prepared nanobio-ink was colloidally stable at least for 7 days (Figure S1 and SI Movie M1).

https://dx.doi.org/10.1021/acsami.0c02596
ACS Appl. Mater. Interfaces 2020, 12, 24231−24241

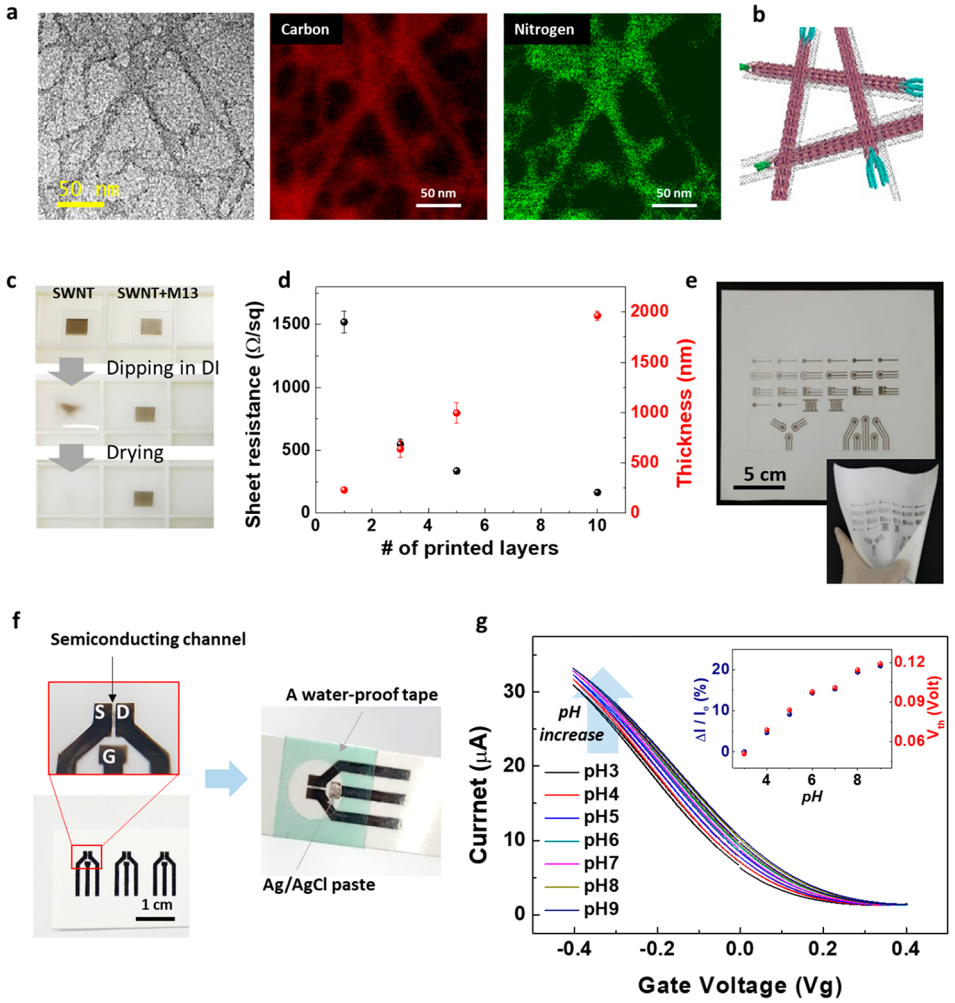

Figure 2. (a) Transmission electron micrographs of the inkjet-printed SWNT−M13 electrode and EF-TEM mapping of the carbon (red) and nitrogen (green) atom, obtained from the same sample shown in the left panel. The green lines indicate the locations of the M13 phage and correlate well with the locations of the high-contrast SWNT lines, suggesting that SWNTs and M13 phage are bound to each other along their lengths within the inkjet-printed nanobio-electrode. (b) Illustration of the binding scheme of M13 phage to SWNT in the inkjet-printed nanobio-electrodes. (c) Hydrostability test result of the inkjet-printed SWNT electrodes using inks without (first column) and with (second column) M13 phage. The SWNT-only electrode readily dissolved upon dipping in DI water and disappeared after one min, illustrating that the M13 phage enhanced the hydrostability of the inkjet-printed electrodes. (d) Dependence of the sheet resistance (left axis) and thickness (right axis) of the SWNT−M13 electrode on the number of print. The molar ratio of SWNT/M13 phage = 10:1. Mean values ± SD were obtained from five different samples. (e) Photographs of the printed SWNT−M13 electrodes on an A4-sized glossy paper in a variety of shapes and geometries. (f) Photographs of the all-inkjet-printed electrochemical field-effect transistors (eFET). S: source, D: drain, G: gate electrodes. SWNT/M13 phage = 10:1 for the electrodes and 2:2 for the semiconducting channel. (g) Transfer characteristics of the eFET measured at various pH conditions. Inset: Changes in the channel current (left axis) and threshold voltage (right axis) as a function of pH.

We first explored rheological parameters of the ink for the single drop formation during the jetting since the formation of satellite drops can cause resolution issues. As an example, the dynamic viscosity of the SWNT−M13 phage solution is presented in Figure 1c. The viscosity of the nanobio-ink increases with the increasing amount of SWNTs and M13 phage. The physical properties of all ink formulations examined in this study are summarized in Table 1 and Figure S2, respectively. Note that the Z number ($Z = (a\rho\gamma)^{1/2}/\eta$ where ρ, γ, η, and a are density, surface tension, viscosity, and characteristic dimension length, respectively) of the inks are higher than 10. It has been reported that the Z number of ink solutions ranging between 1 and 10 is preferred for stable inkjet printing.[22] In some recent studies, single drop formation of ink solutions with $Z > 20$ was successfully demonstrated by adjusting waveforms and firing voltages applied to the piezoelectric component in nozzles.[23−25] However, numerical and phenomenological analyses for the formation of satellite-free droplets with nanobio-inks having a high Z number are unprecedented. In this study, to find optimal jetting conditions of inks with a high Z number, the jetting behavior of the nanobio-ink was systematically simulated using Comsol Multiphysics. The details are described in the SI methods and Figures S3−S5. The simulation result showed that the drop tail velocity exhibited an upper limit for inks of high Z values, and the limit velocity greatly depended on the Z value of the ink (Figure S4). As the Z value was increased, the upper limit of the tail velocity was decreased. This result was consistent with a previous work that reported that the upper limit of Z was determined by the point at which a satellite formed.[26] In our simulation, a single drop was successfully formed when the drop head velocity was lower than a certain

https://dx.doi.org/10.1021/acsami.0c02596
ACS Appl. Mater. Interfaces 2020, 12, 24231−24241

value (Figure S5). With increasing drop head velocity, satellite drops were observed presumably because the tail could not follow the drop head. Therefore, our numerical simulation suggested that the control of the drop head velocity was critical for the single drop formation of the nanobio-ink. This result well matched with the experimental results as presented in Figure 1d and 1e. A single drop was successfully formed when the head velocity of the nanobio-ink was 1.5−5.7 m s^{-1}. These printable ranges well agreed with the value of 5 m s^{-1} predicted by numerical simulation (Figure S5). Therefore, our approach could be used for optimizing jetting conditions of nanoinks when the physical properties of inks cannot be adjusted due to special needs and restrictions.

The inkjet-printing of patterns of nanobio-electrodes were then investigated for device applications. Printing parameters such as drop spacing and number of printing layers were optimized for well-defined dimensions and properties of the electrode on a paper substrate. The surface energy of the paper substrate was estimated to be 57.4 mJ m^{-2} (Figure S6). Isolated drops were observed at a drop spacing wider than 30 μm, whereas an overflow (bulging) occurred at a drop spacing below 10 μm (Figure S7). Drop spacing of 20 μm produced the coalescence of consecutive droplets in a straight line without waving or bulging.[27,28] The minimum feature size and spacing were 75 and 70 μm, respectively (Figure S8). The inkjet-printed electrode on the paper substrate was not detached even using an adhesive tape, confirming its stable adhesion with the paper substrate (Figure S9). The nanostructures and physical properties of the inkjet-printed electrodes were next examined. Transmission electron micrographs of the printed nanobio-electrode are presented in Figure 2a. The micrograph exhibited fine nanonetwork structures with widths ranging from 3 to 10 nm. The high-contrast and sharp lines in the left panel of Figure 2a corresponded to SWNTs. To correlate the locations of the M13 phage, which were also in the one-dimensional shape, carbon atoms (red) and nitrogen (green) were mapped using EF-TEM. The EF-TEM images for carbon and nitrogen are shown in the middle and right panels of Figure 2a. Because only the M13 phage contained nitrogen atoms, the green colors indicated the locations of the M13 phage. The green lines correlated well with the high-contrast SWNT lines shown in the left panel of Figure 2a. These results are consistent with previous results[18] and confirm that the inkjet printing method successfully produces nanobio-networks of SWNT−M13 phage complexes bound to each other along their lengths, as illustrated in Figure 2b. Figure 2c demonstrates that the M13 phage serves as a biological glue to endow the hydrostability of the inkjet-printed electrodes. The inkjet-printed electrode without the M13 phage (depicted as SWNT in Figure 2c) easily dissolved upon dipping in DI water and disappeared after 1 min (first column of Figure 2c) whereas the inkjet-printed electrodes with M13 phage remained stable in an aqueous environment. Surfactants contained in the as-printed electrode were easily washed (Figure S10), producing pure nanobio-electrodes. The Raman spectrum of the inkjet-printed nanonetwork was also analyzed to confirm the quality of the SWNTs after inkjet printing. In the Raman spectrum of SWNTs, the G band, indicative of sp^2 hybridized carbon atoms connected via conjugated double bonds, represents the graphitic nature of SWNTs and the D band implies the presence of defects, such as sp^3, single-bonded carbon atoms, and broken sp^2 bonds in sidewalls. Therefore, structurally defective SWNTs from functionalization or fabrication exhibit a relatively strong peak in the D band in Raman spectra.[29] The Raman spectra of the printed nanobio-electrodes shown in Figure S11 suggest that the SWNTs maintained their structure ($I_D/I_G^+ \approx 1.13\%$)[30] without further defects being generated during the jetting process.

The additive nature of inkjet printing and the tunability of the nanobio-ink composition enabled us to systematically optimize the physical dimensions and properties of the inkjet-printed patterns such as hydrophilicity, thickness, and conductivity. Figure S12 exhibits the dependence of the contact angle on the number of the printed layers. The contact angle decreased with increasing printed layers, implying increased wettability with an increasing printed layer presumably due to the hydrophilic segments of the M13 phages bound to the SWNTs. This enhanced wettability could provide a favorable ionic environment for the electronic materials. Figure 2d shows the dependence of the sheet resistance value and thickness on the number of printed layers. The sheet resistance value of one printed layer of the ink composition of SWNT/M13 phage = 10:1 was 1520 ± 85.9 Ω sq^{-1} and decreased to 164 ± 15.7 Ω sq^{-1} for ten layers. The thickness of one printed layer was 229 ± 27.5 nm, and it linearly increased, producing 1964 ± 48.0 nm for ten printed layers. The electrical resistivity was calculated to be 0.035 ± 0.0024 and 0.032 ± 0.0023 Ω cm for one and ten layers, respectively (Figure S13), which were higher than pure SWNT films by about ten times[31] due to the presence of the electrically insulating biological material, M13 phage. However, it should be noted that these values are low enough to provide conductive electrodes for transistors and enzymatic biosensors and enable efficient electrochemical coupling between the nanostructured electrode and enzyme. A variety of electrodes with versatile configurations and thickness were successfully fabricated on an A4-sized paper (Figure 2e), confirming the additive and controllable patterning capability of inkjet-printing to produce nanobio-electrodes in a large scale without using any prepatterned mask. The lighter color indicates a thinner thickness of the pattern.

Controlling the ink composition can further produce electrodes with different electronic transport behavior such as semiconductors. This capability can provide an all-inkjet-printed active device such as transistors. As a demonstration, an all-inkjet-printed electrochemical field-effect transistor (eFET) was fabricated as shown in Figure 2f. The source (S), drain (D), and gate (G) electrodes of the eFET are indicated. Ten layers of a molar ratio of SWNT/M13 phage = 10:1 were inkjet-printed for electrodes, and a single layer of a nanobio-ink of a molar ratio of SWNT/M13 phage = 2:2 was inkjet-printed for the channel. The size of the S and D electrodes was 2 mm (H) × 1 mm (W), and the S and D electrodes were separated by 300 μm. The molar ratio of SWNT/M13 phage = 2:2 was chosen based on our previous reports.[18,32] The printed gate electrode was coated with Ag/AgCl paste (ALS. Co., Ltd.) for applying a stable gate bias (Figure S14). The transfer characteristics and output curves of the eFET were measured after dropping 10 μL of 10 mM phosphate-citrate buffer in the open region of the water-proof tape. The results are summarized in Figures 2g and S15. The transfer curve clearly indicated that the all-inkjet-printed eFET device using SWNT−M13 phage ink successfully behaved as a p-type transistor. The $I_{Vg=-0.4\ V}/I_{Vg=0.2\ V}$ was ∼25. This low ratio and the nonsaturating behavior of the output curves

https://dx.doi.org/10.1021/acsami.0c02596
ACS Appl. Mater. Interfaces 2020, 12, 24231−24241

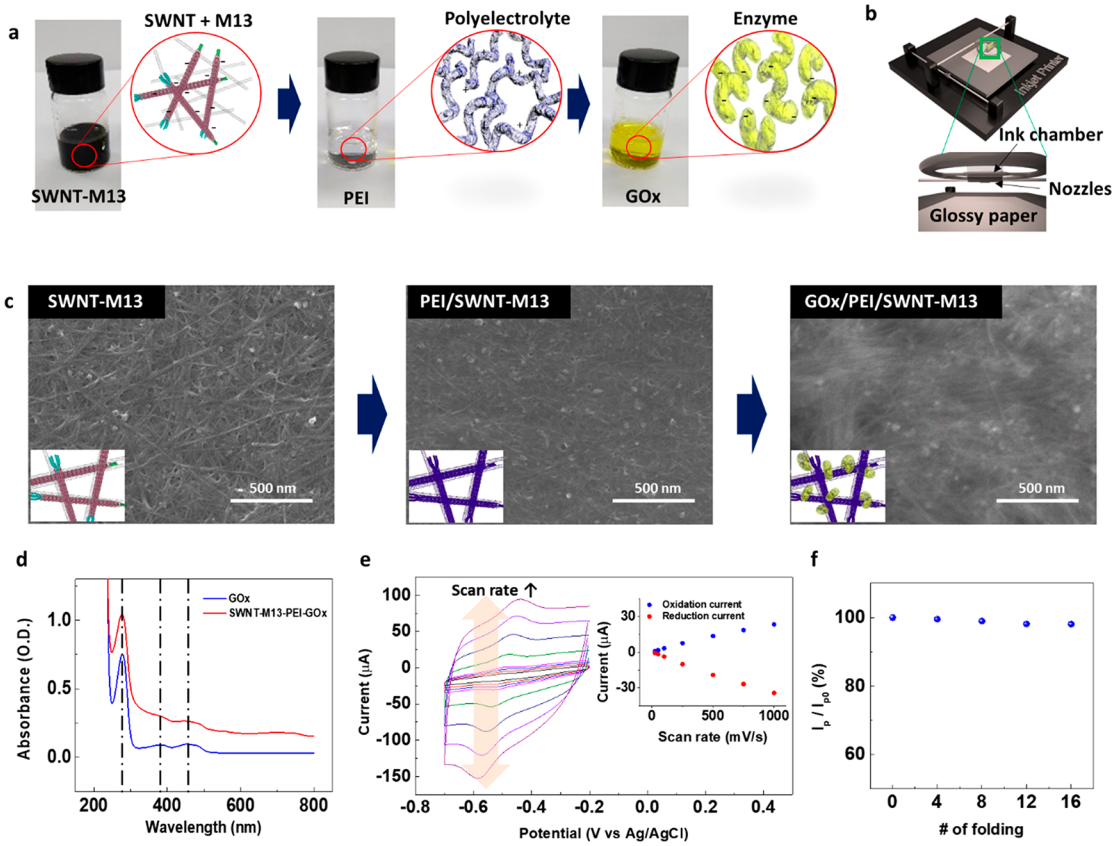

Figure 3. (a) Illustration of the sequential inkjet printing process of various types of ink solutions. Three inks were sequentially inkjet-printed: SWNT−M13 ink, polyelectrolytes, and then enzyme solutions. Photographs and illustrations of the key components with appropriate surface charge states of each ink solution are shown. (b) Schematic illustration of inkjet printing on a glossy paper using the developed inks. (c) Scanning electron micrographs of the inkjet-printed electrodes after printing each ink solution for the fabrication of the enzymatic glucose biosensor. Inset: Illustrations of the binding scheme of the components after each printing step. (d) UV−Vis absorption spectra of the pristine GOx and the inkjet-printed enzymatic electrode, GOx/PEI/SWNT−M13. The shift of the polypeptide was 1 nm, and the two peaks of 377 and 458 nm that were related to FAD/$FADH_2$ moiety were 1 and 2 nm, respectively, indicating that the conformational changes by the inkjet printing process were small. (e) CV curves of the enzyme electrode measured at various scan rates. The clear redox peaks indicated excellent electrochemical coupling of the GOx enzyme with the electrode. Inset: Oxidation and reduction currents after subtraction of background capacitive currents. Linearly increased currents with increasing scan rate indicated the surface-controlled process of immobilized enzymes. (f) Change in the reduction peak current upon repeated complete folding up to 16 times. Mean values ± SD were obtained from three different samples.

(Figure S15) were due to the randomly oriented SWNT network channels with high coverage.[33] The leakage current level of the eFET was negligible and the time constant of the electrochemical processes was estimated to be ∼200 ms (Figure S16).

The transfer curves were shifted to a more positive potential, and the source-drain current (I_{SD}) was accordingly increased upon a gradual increase in pH of the buffer solution from 3 to 9. Both the V_{th} shift and I_{SD} increase were ascribed to the increase of the hole concentration in the p-type channel due to enhanced negative polarization of M13 phage.[32] As the IEP of M13 phage is known to be ∼4,[32] the carboxyl functional groups of the peptides on the body of the M13 phage were deprotonated as the pH of the electrolytes was gradually increased from 3 to 9. The increased negative polarization of the M13 phage induced more positive carriers in the SWNT channel, resulting in the V_{th} shift and I_{SD} increase. The V_{th} shift was estimated to be 12 mV pH^{-1}, and the I_{SD} current was increased by 20% as the pH increased from 3 to 9 (Inset of Figure 2g). The electrolyte-gating response of the SWNT−M13 phage channel indicates strong electrochemical coupling of the printed nanobio-devices.

In addition to the amphiphilic nanobio-inks, various other solutions can be further combined to produce different types of devices that require efficient electrochemical couplings of nanobio-electrodes in aqueous solutions such as all-inkjet-printed enzymatic biosensors. As a demonstration, different types of inks were employed in addition to the nanobio-ink of SWNT/ M13 phage = 10:1 such as 5% w/v polyethylenimine (PEI) in water and 25 mg mL^{-1} GOx in 10 mM PBS, as shown in Figure 3a. In this study, the glucose oxidase (GOx) enzyme was chosen based on both the tremendous impact of high-performance glucose sensors in the new healthcare market and the challenges of obtaining intimate electrical coupling of GOx enzymes in a biocompatible and simple manner.[34,35] Viscosity, surface tension, and the calculated Z number of each ink solution used for the all-inkjet-printed glucose biosensor are summarized in Table 1. The inkjet-printing conditions for all the ink solutions are summarized in the SI Table S1. Figure 3a and 3b schematically illustrates the full sequential printing processes for the fabrication of the all-inkjet-printed glucose sensor. Ten layers of the SWNT−M13 phage nanonetwork were printed using the ink of SWNT/M13 phage = 10:1 to produce working (W), counter (C), and reference (R)

https://dx.doi.org/10.1021/acsami.0c02596
ACS Appl. Mater. Interfaces 2020, 12, 24231−24241

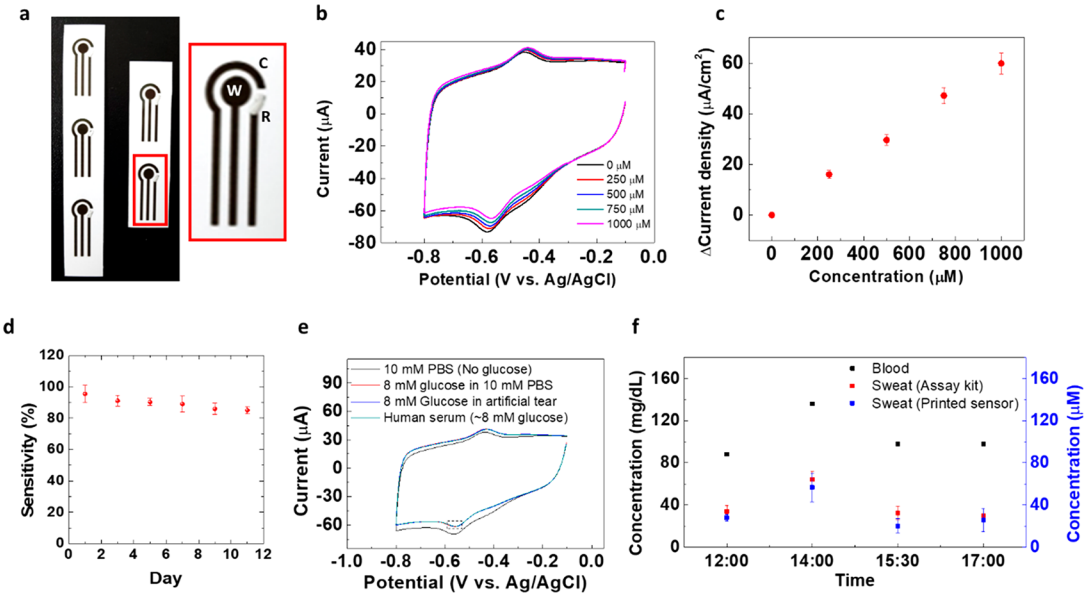

Figure 4. (a) Photograph of five all-inkjet-printed enzymatic biosensors. W: working, C: counter and R: reference electrodes. The gap between the C and W electrodes is ∼1 mm. The R electrode was coated with Ag/AgCl paste. (b) CV curves measured in buffer solutions containing various glucose concentrations. Cathodic current decreases with increasing glucose concentration. (c) Changes in the cathodic peak current density with increasing glucose concentration. The sensitivity value was ∼56.07 ± 2.473 μA mM^{-1} cm^{-2}. Mean values ± SD were calculated from three different samples. (d) Stability of the all-inkjet-printed glucose sensor. Mean values ± SD were calculated from three different samples. (e) CV curves measured in various physiological solutions, such as buffer solution (PBS), human serum, and artificial tear solution. (f) Comparison of blood glucose levels (left axis) measured using a commercial glucometer with sweat glucose levels measured using the developed all-inkjet-printed biosensor and the commercial glucose assay kit. The developed electrochemical glucose sensor matched well with the assay kit, and the sweat glucose levels correlated well with the blood glucose levels (correlation factor: 0.671, the ratio of the sweat glucose level (μM) to the blood glucose level (mg/dL), R^2=0.77). Mean values ± SD of the sweat glucose level were calculated from three different samples.

electrodes with high conductivity and ionic compatibility. Note that the printed electrodes were negatively charged due to the negative surface charge of M13 phage (IEP ≈ 4). After washing residual surfactants using DI water, one layer of a positively charged PEI (IEP ≈ 10) ink was printed only onto the W electrode located at the center of the biosensors, and then ten layers of negatively charged GOx enzyme solution (IEP ≈ 4.3) were inkjet-printed onto the PEI-coated W electrode. Scanning electron micrographs of the corresponding electrodes after printing of each type of ink solution are shown in Figure 3c. The micrographs show fine nanonetwork structures of the printed base electrode (SWNT−M13) and also suggest that the subsequent PEI and enzyme layers were well coated. The binding scheme of the components after each printing step is illustrated in the inset.

A key factor for making highly sensitive enzymatic biosensors is efficiently coupling enzymes with electrodes, preserving the catalytic activity of the enzymes after their immobilization. Many studies have shown that the catalytic activity of enzymes can be easily degraded for the enzymatic biosensors fabricated using either thermal- or piezo-based inkjet printers[36,37] because harsh temperature- or pressure-induced jetting conditions can cause a structural change of the enzymes. Therefore, the possible conformational change of inkjet-printed GOx in this study was investigated by absorption spectrum analysis (Figure 3d). The UV−Vis spectrum of the native GOx (red curve) exhibited three well-defined peaks at 280, 377, and 458 nm. The peak at 280 nm corresponds to polypeptide chains of GOx, and peaks at 377 and 458 nm correspond to the flavin adenine dinucleotide (FAD/$FADH_2$) moiety of GOx, respectively. The shift of the polypeptide after inkjet-printing was 1 nm, and the two peaks of 377 and 458 nm that were related to FAD/$FADH_2$ moiety were 1 and 2 nm, respectively, indicating that the conformational changes were small,[38−40] presumably due to the mild jetting condition of GOx ink used in this study such as low firing voltage of 30 V.[36]

The electrical coupling within the inkjet-printed enzymatic nanostructured electrodes was then examined by CV measurement in 10 mM PBS solution. The CV curves showed both strong cathodic and anodic redox peaks in the negative potential ranges, and these peaks were ascribed to the electron transfer (ET) process of the FAD/$FADH_2$ redox cofactor of immobilized GOx (Figures 3e, S17, and S18).[41−44] For the analysis of the surface coverage of GOx and the rate constant, k_s, of ET, the background capacitive currents were subtracted. The surface concentration of immobilized GOx was estimated according to $\Gamma = Q/nFA$ where Q is the charge, n is the number of transferred electrons, F is the Faraday constant, and A is the geometric surface area of the working electrode. The estimated surface concentration of GOx was 3.49 × 10^{-10} mol cm^{-2}, which was higher than the theoretical value (2.86 × 10^{-12} mol cm^{-2}) of monolayer GOx (Stokes radius, 4.3 nm) on bare gold electrodes[45] and the literature values (∼10^{-10} mol cm^{-2}) of the electrodes employing nanomaterials.[41,46] This implies that the developed nanobio-electrodes in this study provided a large effective surface area for the enzymes. Figures 3e (inset) and S17 also show that the oxidation and reduction currents after subtraction of background capacitive currents linearly increased as the scan rate increased from 25 to 1000 mV s^{-1}, indicating the surface-controlled process of immobilized enzymes. On the basis of Laviron's equation, the heterogeneous ET rate constant (k_s) was estimated to be 3.4 s^{-1}, indicating that the SWNT−M13 hybrid electrode provided enzymes with intimate electrical contacts within the inkjet-

https://dx.doi.org/10.1021/acsami.0c02596
ACS Appl. Mater. Interfaces 2020, 12, 24231−24241

printed enzyme electrodes. The reversible FAD/$FADH_2$ redox peaks of the paper-based glucose biosensor were well retained even upon 90° folding and repeated complete folding, as shown in Figures 3f and S19. The change in reduction peak current after complete folding 16 times was ∼1.9%. These stable operation upon folding would be presumably due to the high mechanical stability of the SWNT−M13 hybrid electrode enabled by the M13 phage and the bio/chemical-compatibility of papers. All these results suggest the feasibility of all-inkjet-printed high-performance flexible biosensors.

The all-inkjet-printed enzymatic biosensor was used for analyzing sweat glucose levels. Five all-inkjet-printed enzymatic glucose sensors are shown in Figure 4a. Here, it is worth noting that the diameter of the W electrode was 4 mm, and it was separated from the surrounding C and R electrodes over a distance less than 1 mm. Furthermore, PEI and GOx inks were only superimposed on the center of the working electrode. In such a spatial resolution, a solution processing (i.e., drop-casting) for the enzyme immobilization would not be feasible, particularly on a paper substrate. These results confirmed the advantages of inkjet printing such as the multiple productions of identical image layers with high reliability, resolution, and reproducibility. The sweat glucose levels are known to be lower than 0.5 mM, which is much lower than the blood glucose levels ranging over several mM.[35] Therefore, the sensing characteristics of the all-inkjet-printed glucose biosensors were examined in an air-saturated PBS solution containing a variety of glucose concentrations from 0 to 1000 μM. To obtain high sensitivity, ten layers of GOx inks were inkjet printed (Figure S20). Figures 4b and S21 show that the cathodic peak current decreased and the anodic peak current increased with increasing glucose concentration. In contrast, the CV curves of the inkjet-printed electrode without the GOx layer did not change upon the addition of glucose (Figure S22). The dependence of the peak current on the glucose concentration of the developed biosensor was ascribed to (1) the increased amount of the reduced form of FAD by the following enzymatic reaction, GOx (FAD) + Glucose → GOx ($FADH_2$) + Gluconolactone, and (2) the decrease in the extent of the cathodic reaction with dissolved O_2 that was enzymatically consumed by the $FADH_2$.[20,41−44] The change in the cathodic peak current level was used to calculate the sensitivity of the glucose sensor. The sensitivity of the all-inkjet-printed glucose sensor was 56.07 ± 2.473 $\mu A\ mM^{-1}\ cm^{-2}$ and the limit of detection (LOD) was 20 μM. The LOD was calculated using the equation: LOD = 3 × standard deviation of the peak current (n = 10)/sensitivity.[47] The apparent Michaelis−Menten constant (K_{app}^{m}) of the all-inkjet-printed glucose biosensor was estimated to be 887 μM using the electrochemical version of the Lineweaver−Burk equation (Figure S23). A low value of 887 μM of the all-inkjet-printed glucose biosensor suggests that the enzyme electrode possessed high affinity, as well as high enzyme catalytic activity toward glucose molecules.[48−51]

The long-term stability was also studied by storing the all-inkjet-printed glucose sensors in a refrigerator at 4 °C, and the measurements proceeded every 2 days up to 11 days. During the first 5 days, 90% of the initial sensitivity was maintained, and 85% of the initial sensitivity was retained after 11 days (Figure 4d). The selectivity of the glucose sensor was examined using various physiological solutions, such as human serum and artificial tear solution. The cathodic and anodic peaks measured in these physiological solutions differed by under 1.4% from the peak currents measured in the PBS solution containing 10 mM glucose, as shown in Figure 4e. The excellent selective operation was ascribed to the negative potential range (<−200 mV vs Ag/AgCl) of glucose biosensors that effectively avoided the oxidation reactions of interfering substances, such as ascorbic acid, uric acid, and acetaminophen (Figure S24).[3,20] Although various materials and types of biosensors have been proposed through printing processes for realizing highly sensitive biosensors,[52−54] including printed carbon nanotubes on paper substrates for detecting hydrogen peroxide,[55] printed graphene electrodes with enzymes on flexible substrates for detecting glucose,[56] and printed Prussian blue nanoparticle-modified electrodes for detecting cholesterol,[57] a more challenging type of biosensor, such as direct electron transfer (DET)-based biosensors has not yet been reported using printing methods. The successful realization of the all-inkjet-printed DET-based biosensor in this study implies excellent electrochemical coupling of the enzymes with electrodes and confirms the advantages of our approach.

Sweat glucose levels were next monitored using the all-inkjet-printed glucose sensor. The study was performed based on the regulation of the institutional review board (IRB) of the Korea Institute of Science and Technology (KIST, IRB#:2016−024). Two healthy, 24-year-old male volunteers with no medical history of heart or diabetes problems participated in this study. The blood and sweat samples were collected every 90−120 min from 12:00 pm to 5:00 pm. The blood glucose levels were measured using a commercial glucometer (CareSens N Premier Inc., Korea), and the sweat glucose levels were measured using both a glucose assay kit (Sigma-Aldrich) and the all-inkjet-printed glucose biosensors. The calibration curve of the all-inkjet-printed glucose biosensors for calculating the sweat glucose levels is presented in Figure S25. The results from all three different types of sensors are summarized in Figure 4f. The glucose levels in sweat and blood significantly increased after a lunch meal was provided to the volunteers at 12:30 pm. The sweat glucose levels measured by the all-inkjet-printed glucose sensor were quite well-matched with the assay kit, and changes in the sweat glucose levels were well correlated with the trends in the blood glucose levels (correlation factor: 0.671, the ratio of the sweat glucose concentration (μM) to the blood glucose concentration (mg/dL), R^2 = 0.77). In the future, the combination of the all-inkjet-printed biosensor technology with sweat control could be further exploited to provide wearable biosensors for continuous monitoring of biofluids.[58] Altogether, these results suggest the great potential of an all-inkjet-printed biosensor using nanobio-ink for point-of-care, personalized medicine, and digital healthcare.

CONCLUSIONS

Here, we have demonstrated all-inkjet-printed nanobio-devices with efficient electrochemical coupling as well as strong hydrostability and tunable electrical and chemical properties. The amphiphilic biomaterial, M13 phage, not only stabilized the inkjet-printed nanostructured electrode in an aqueous environment but also provided ionic compatibility to the electrodes. Controlling the nanobio-ink formulation with the same components also allowed for versatile electrical properties of the printed patterns. Electrodes with various configurations and thicknesses were successfully fabricated on an A4-sized paper in a large scale without using any prepatterned masks. All-inkjet-printed eFETs successfully

https://dx.doi.org/10.1021/acsami.0c02596
ACS Appl. Mater. Interfaces 2020, 12, 24231−24241

exhibited pH-sensitive electrical current modulation. Moreover, highly sensitive, selective, and mechanically stable all-inkjet-printed glucose biosensors successfully detected sweat glucose levels. The broad substrate selection, precise spatial control, high reproducibility, and additive and direct patterning capability of inkjet printing and its combination with functional biomaterials enabling directed assembly hold great promise for biointegrated electronics for personalized medicine, digital healthcare, and emerging biomimetic devices.

■ ASSOCIATED CONTENT

Supporting Information

The Supporting Information is available free of charge at https://pubs.acs.org/doi/10.1021/acsami.0c02596.

Detailed description of the numerical simulation; absorption curve of the nanobio-ink; physical properties of formulated inks; axis symmetry geometry and boundary conditions of the modeled nozzle; simulated drop tail and head velocities for ink solutions of different Z values; numerical simulation results for drop head velocity jetted at various conditions; surface energy of the paper substrate; effect of drop spacing on morphologies of printed nanobio-inks on a glossy paper; minimum feature size and spacing; adhesion of the printed nanobio-ink with the paper substrate; scanning electron micrographs of the inkjet-printed and SWNT−M13 electrode before and after washing; Raman spectra of the inkjet-printed SWNT−M13 electrode; dependence of the contact angle of the SWNT−M13 electrode on the number of print; dependence of the resistivity of the inkjet-printed electrodes on the number of print; stable operation of the gate electrode coated with Ag/AgCl paste; output curves of the all-inkjet-printed eFET; leakage current and time constant of the eFET; CV curves after subtraction of background capacitive currents; effect of the buffer condition on the all-printed electrode in N_2-saturated 10 mM PBS buffer and air-saturated 10 mM PBS buffer; CV curves measured from the paper-based biosensor before and after bending by 90°; effect of the number of printed layer of GOx; CV curves of the SWNT−M13 electrode without GOx measured in various glucose concentrations; Lineweaver−Burk plot for catalyzed glucose electro-oxidation on the SWNT−M13-PEI-GOx sensor; high selectivity of the all-inkjet-printed glucose sensors; and calibration curve of the all-inkjet-printed glucose sensor used for calculating the sweat glucose level; parameters used for inkjet-printing of all the functional inks used in this study (PDF)

Movie showing jetting of the nanobio-ink stored for 7 days after preparation (MP4)

■ AUTHOR INFORMATION

Corresponding Authors

Hyunjung Yi − *Post-Silicon Semiconductor Institute, Korea Institute of Science and Technology, Seoul 02792, Republic of Korea;* orcid.org/0000-0001-8812-497X; Email: hjungyi@kist.re.kr

In-Suk Choi − *Department of Materials Science and Engineering, Seoul National University, Seoul 08826, Republic of Korea;* orcid.org/0000-0002-5933-7551; Email: insukchoi@snu.ac.kr

Woong-Ryeol Yu − *Department of Materials Science and Engineering, Seoul National University, Seoul 08826, Republic of Korea;* orcid.org/0000-0001-5916-3339; Email: woongryu@snu.ac.kr

Authors

Tae-Hyung Kang − *Post-Silicon Semiconductor Institute, Korea Institute of Science and Technology, Seoul 02792, Republic of Korea; Department of Materials Science and Engineering, Seoul National University, Seoul 08826, Republic of Korea*

Seung-Woo Lee − *Department of Fine Chemistry, Seoul National University of Science and Technology, Seoul 01811, Republic of Korea;* orcid.org/0000-0003-4627-4712

Kyowook Hwang − *Department of Fine Chemistry, Seoul National University of Science and Technology, Seoul 01811, Republic of Korea*

Wonbo Shim − *Department of Materials Science and Engineering, Seoul National University, Seoul 08826, Republic of Korea*

Ki-Young Lee − *Post-Silicon Semiconductor Institute, Korea Institute of Science and Technology, Seoul 02792, Republic of Korea;* orcid.org/0000-0002-9327-2026

Jung-Ah Lim − *Post-Silicon Semiconductor Institute, Korea Institute of Science and Technology, Seoul 02792, Republic of Korea;* orcid.org/0000-0002-3007-3855

Complete contact information is available at: https://pubs.acs.org/10.1021/acsami.0c02596

Author Contributions

The manuscript was written through contributions of all authors. All authors have given approval to the final version of the manuscript. T.-H.K. and S.-W.L. contributed equally to this work.

Notes

The authors declare no competing financial interest.

■ ACKNOWLEDGMENTS

This work was supported by the New Faculty Startup Fund from Seoul National University. This work was also supported by Korea Institute of Science and Technology (KIST) through Young Fellow Program and Institutional Program. This work was also supported by the National Research Foundation of Korea funded by the Ministry of Science and ICT (Grant No. NRF-2015M3A9E2030105, NRF-2017R1C1B2004765, and NRF-2018M3A7B4071106).

■ ABBREVIATIONS USED

SWNT = single-walled carbon nanotube
SC = sodium cholate
TBS = tris-buffered saline
PEI = polyethyleneimine
DI = deionized
GOx = glucose oxidase
PBS = phosphate-buffered saline
EF-TEM = Energy-filtered transmission electron microscopy
FAD = flavin adenine dinucleotide
IEP = isoelectric point

■ REFERENCES

(1) Lanzani, G. Organic Electronics Meets Biology. *Nat. Mater.* **2014**, *13*, 775−776.

(2) Oh, D.; Qi, J.; Lu, Y.-C.; Zhang, Y.; Shao-Horn, Y.; Belcher, A. M. Biologically Enhanced Cathode Design for Improved Capacity and Cycle Life for Lithium-Oxygen Batteries. *Nat. Commun.* **2013**, *4*, 2756.
(3) Lee, S.-W.; Lee, K.-Y.; Song, Y.-W.; Choi, W. K.; Chang, J.; Yi, H. Direct Electron Transfer of Enzymes in a Biologically Assembled Conductive Nanomesh Enzyme Platform. *Adv. Mater.* **2016**, *28* (8), 1577−1584.
(4) Cui, Y. Engineered Phages for Electronics. *Biosens. Bioelectron.* **2016**, *85*, 964−976.
(5) Wang, L.; Zhang, Y.; Wu, A.; Wei, G. Designed Graphene-Peptide Nanocomposites for Biosensor Applications: A review. *Anal. Chim. Acta* **2017**, *985*, 24−40.
(6) Li, D.; Zhang, W.; Yu, X.; Wang, Z.; Su, Z.; Wei, G. When Biomolecules Meet Graphene: From Molecular Level Interactions to Material Design and Applications. *Nanoscale* **2016**, *8* (47), 19491−19509.
(7) Green, N. S.; Norton, M. L. Interactions of DNA with Graphene and Sensing Applications of Graphene Field-Effect Transistor Devices: A Review. *Anal. Chim. Acta* **2015**, *853*, 127−142.
(8) Teengam, P.; Siangproh, W.; Tuantranont, A.; Henry, C. S.; Vilaivan, T.; Chailapakul, O. Electrochemical Paper-Based Peptide Nucleic Acid Biosensor for Detecting Human Papillomavirus. *Anal. Chim. Acta* **2017**, *952*, 32−40.
(9) Lee, K.; Yoo, Y. K.; Chae, M.-S.; Hwang, K. S.; Lee, J.; Kim, H.; Hur, D.; Lee, J. H. Highly Selective Reduced Graphene Oxide (rGO) Sensor Based on a Peptide Aptamer Receptor for Detecting Explosives. *Sci. Rep.* **2019**, *9* (1), 10297.
(10) Li, J.; Rossignol, F.; Macdonald, J. Inkjet Printing for Biosensor Fabrication: Combining Chemistry and Technology for Advanced Manufacturing. *Lab Chip* **2015**, *15* (12), 2538−2558.
(11) Whaley, S. R.; English, D. S.; Hu, E. L.; Barbara, P. F.; Belcher, A. M. Selection of Peptides with Semiconductor Binding Specificity for Directed Nanocrystal Assembly. *Nature* **2000**, *405* (6787), 665−668.
(12) Sarikaya, M.; Tamerler, C.; Jen, A. K. Y.; Schulten, K.; Baneyx, F. Molecular Biomimetics: Nanotechnology through Biology. *Nat. Mater.* **2003**, *2* (9), 577−585.
(13) Wang, S.; Humphreys, E. S.; Chung, S.-Y.; Delduco, D. F.; Lustig, S. R.; Wang, H.; Parker, K. N.; Rizzo, N. W.; Subramoney, S.; Chiang, Y.-M.; Jagota, A. Peptides with Selective Affinity for Carbon Nanotubes. *Nat. Mater.* **2003**, *2* (3), 196−200.
(14) Lee, Y. J.; Yi, H.; Kim, W.-J.; Kang, K.; Yun, D. S.; Strano, M. S.; Ceder, G.; Belcher, A. M. Fabricating Genetically Engineered High-Power Lithium-Ion Batteries Using Multiple Virus Genes. *Science* **2009**, *324* (5930), 1051−1055.
(15) Yi, H.; Ghosh, D.; Ham, M.-H.; Qi, J.; Barone, P. W.; Strano, M. S.; Belcher, A. M. M13 Phage-Functionalized Single-Walled Carbon Nanotubes As Nanoprobes for Second Near-Infrared Window Fluorescence Imaging of Targeted Tumors. *Nano Lett.* **2012**, *12* (3), 1176−1183.
(16) Dang, X.; Yi, H.; Ham, M.-H.; Qi, J.; Yun, D. S.; Ladewski, R.; Strano, M. S.; Hammond, P. T.; Belcher, A. M. Virus-Templated Self-Assembled Single-Walled Carbon Nanotubes for Highly Efficient Electron Collection in Photovoltaic Devices. *Nat. Nanotechnol.* **2011**, *6*, 377−384.
(17) Oh, D.; Dang, X.; Yi, H.; Allen, M. A.; Xu, K.; Lee, Y. J.; Belcher, A. M. Graphene Sheets Stabilized on Genetically Engineered M13 Viral Templates as Conducting Frameworks for Hybrid Energy-Storage Materials. *Small* **2012**, *8* (7), 1006−1011.
(18) Lee, K.-Y.; Byeon, H.-H.; Jang, C.; Choi, J.-H.; Choi, I.-S.; Jung, Y.; Kim, W.; Chang, J.; Yi, H. Hydrodynamic Assembly of Conductive Nanomesh of Single-Walled Carbon Nanotubes Using Biological Glue. *Adv. Mater.* **2015**, *27* (5), 922−928.
(19) Ju, S.; Lee, K.-Y.; Min, S.-J.; Yoo, Y. K.; Hwang, K. S.; Kim, S. K.; Yi, H. Single-Carbon Discrimination by Selected Peptides for Individual Detection of Volatile Organic Compounds. *Sci. Rep.* **2015**, *5*, 9196.
(20) Lee, S.-W.; Kang, T.-H.; Lee, S. K.; Lee, K.-Y.; Yi, H. Hydrodynamic Layer-by-Layer Assembly of Transferable Enzymatic Conductive Nanonetworks for Enzyme-Sticker-Based Contact Printing of Electrochemical Biosensors. *ACS Appl. Mater. Interfaces* **2018**, *10* (42), 36267−36274.
(21) Kyte, J.; Doolittle, R. F. A Simple Method for Displaying the Hydropathic Character of a Protein. *J. Mol. Biol.* **1982**, *157* (1), 105−132.
(22) Reis, N.; Ainsley, C.; Derby, B. Ink-jet Delivery of Particle Suspensions by Piezoelectric Droplet Ejectors. *J. Appl. Phys.* **2005**, *97* (9), 094903.
(23) McManus, D.; Vranic, S.; Withers, F.; Sanchez-Romaguera, V.; Macucci, M.; Yang, H.; Sorrentino, R.; Parvez, K.; Son, S.-K.; Iannaccone, G.; Kostarelos, K.; Fiori, G.; Casiraghi, C. Water-Based and Biocompatible 2D Crystal Inks for All-Inkjet-Printed Heterostructures. *Nat. Nanotechnol.* **2017**, *12*, 343−350.
(24) Shin, P.; Sung, J.; Lee, M. H. Control of Droplet Formation for Low Viscosity Fluid by Double Waveforms Applied to a Piezoelectric Inkjet Nozzle. *Microelectron. Reliab.* **2011**, *51* (4), 797−804.
(25) Torrisi, F.; Hasan, T.; Wu, W.; Sun, Z.; Lombardo, A.; Kulmala, T. S.; Hsieh, G.-W.; Jung, S.; Bonaccorso, F.; Paul, P. J.; Chu, D.; Ferrari, A. C. Inkjet-Printed Graphene Electronics. *ACS Nano* **2012**, *6* (4), 2992−3006.
(26) Jang, D.; Kim, D.; Moon, J. Influence of Fluid Physical Properties on Ink-Jet Printability. *Langmuir* **2009**, *25* (5), 2629−2635.
(27) Gao, M.; Li, L.; Song, Y. Inkjet Printing Wearable Electronic Devices. *J. Mater. Chem. C* **2017**, *5* (12), 2971−2993.
(28) Stringer, J.; Derby, B. Formation and Stability of Lines Produced by Inkjet Printing. *Langmuir* **2010**, *26* (12), 10365−10372.
(29) Kabbani, M. A.; Tiwary, C. S.; Autreto, P. A. S.; Brunetto, G.; Som, A.; Krishnadas, K. R.; Ozden, S.; Hackenberg, K. P.; Gong, Y.; Galvao, D. S.; Vajtai, R.; Kabbani, A. T.; Pradeep, T.; Ajayan, P. M. Ambient Solid-State Mechano-Chemical Reactions between Functionalized Carbon Nanotubes. *Nat. Commun.* **2015**, *6* (1), 7291.
(30) Tachibana, M. Characterization of Laser-Induced Defect Sand Modification in Carbon Nanotubes by Raman Spectroscopy. In *Physical and Chemical Properties of Carbon Nanotubes*; Tachibana, M., Ed.; InTech: Rijeka, 2013; pp 31−52.
(31) Bekyarova, E.; Itkis, M. E.; Cabrera, N.; Zhao, B.; Yu, A.; Gao, J.; Haddon, R. C. Electronic Properties of Single-Walled Carbon Nanotube Networks. *J. Am. Chem. Soc.* **2005**, *127* (16), 5990−5995.
(32) Byeon, H.-H.; Lee, S.-W.; Lee, E.-H.; Kim, W.; Yi, H. Biologically Templated Assembly of Hybrid Semiconducting Nanomesh for High Performance Field Fffect Transistors and Sensors. *Sci. Rep.* **2016**, *6*, 35591.
(33) Cao, Q.; Rogers, J. A. Ultrathin Films of Single-Walled Carbon Nanotubes for Electronics and Sensors: A Review of Fundamental and Applied Aspects. *Adv. Mater.* **2009**, *21*, 29−53.
(34) Gao, W.; Emaminejad, S.; Nyein, H. Y. Y.; Challa, S.; Chen, K.; Peck, A.; Fahad, H. M.; Ota, H.; Shiraki, H.; Kiriya, D.; Lien, D.-H.; Brooks, G. A.; Davis, R. W.; Javey, A. Fully Integrated Wearable Sensor Arrays for Multiplexed in situ Perspiration Analysis. *Nature* **2016**, *529* (7587), 509−514.
(35) Lee, H.; Choi, T. K.; Lee, Y. B.; Cho, H. R.; Ghaffari, R.; Wang, L.; Choi, H. J.; Chung, T. D.; Lu, N.; Hyeon, T.; Choi, S. H.; Kim, D.-H. A Graphene-Based Electrochemical Device with Thermoresponsive Microneedles for Diabetes Monitoring and Therapy. *Nat. Nanotechnol.* **2016**, *11*, 566−572.
(36) Cook, C. C.; Wang, T.; Derby, B. Inkjet Delivery of Glucose Oxidase. *Chem. Commun.* **2010**, *46* (30), 5452−5454.
(37) Nishioka, G. M.; Markey, A. A.; Holloway, C. K. Protein Damage in Drop-on-Demand Printers. *J. Am. Chem. Soc.* **2004**, *126* (50), 16320−16321.
(38) Zhang, X.; Liu, D.; Li, L.; You, T. Direct Electrochemistry of Glucose Oxidase on Novel Free-Standing Nitrogen-Doped Carbon Nanospheres@Carbon Nanofibers Composite Film. *Sci. Rep.* **2015**, *5* (1), 9885.

https://dx.doi.org/10.1021/acsami.0c02596
ACS Appl. Mater. Interfaces 2020, 12, 24231−24241

(39) Xu, X.; Wu, P.; Xu, W.; Shao, Q.; An, L.; Zhang, H.; Cai, C.; Zhao, B. Effects of Guanidinium Ions on the Conformational Structure of Glucose Oxidase Studied by Electrochemistry, Spectroscopy, and Theoretical Calculations: Towards Developing a Chemical-Induced Protein Conformation Assay. *Phys. Chem. Chem. Phys.* **2012**, *14* (16), 5824−5836.
(40) Shao, Q.; Wu, P.; Xu, X.; Zhang, H.; Cai, C. Insight into the Effects of Graphene Oxide Sheets on the Conformation and Activity of Glucose Oxidase: Towards Developing a Nanomaterial-Based Protein Conformation Assay. *Phys. Chem. Chem. Phys.* **2012**, *14* (25), 9076−9085.
(41) Deng, C.; Chen, J.; Nie, Z.; Si, S. A Sensitive and Stable Biosensor Based on the Direct Electrochemistry of Glucose Oxidase Assembled Layer-By-Layer at the Multiwall Carbon Nanotube-Modified Electrode. *Biosens. Bioelectron.* **2010**, *26* (1), 213−219.
(42) Liang, T.; Zou, L.; Guo, X.; Ma, X.; Zhang, C.; Zou, Z.; Zhang, Y.; Hu, F.; Lu, Z.; Tang, K.; Li, C. M. Rising Mesopores to Realize Direct Electrochemistry of Glucose Oxidase toward Highly Sensitive Detection of Glucose. *Adv. Funct. Mater.* **2019**, *29* (44), 1903026.
(43) Min, K.-I.; Lee, S.-W.; Lee, E.-H.; Lee, Y.-S.; Yi, H.; Kim, D.-P. Facile Nondestructive Assembly of Tyrosine-Rich Peptide Nanofibers as a Biological Glue for Multicomponent-Based Nanoelectrode Applications. *Adv. Funct. Mater.* **2018**, *28* (11), 1705729.
(44) Guo, C. X.; Li, C. M. Direct Electron Transfer of Glucose Oxidase and Biosensing of Glucose on Hollow Sphere-Nanostructured Conducting Polymer/Metal Oxide Composite. *Phys. Chem. Chem. Phys.* **2010**, *12* (38), 12153−12159.
(45) Jin-Zhong, X.; Jun-Jie, Z.; Qiang, W.; Zheng, H.; Hong-Yuan, C. Direct Electron Transfer between Glucose Oxidase and Multiwalled Carbon Nanotubes. *Chin. J. Chem.* **2003**, *21* (8), 1088−1091.
(46) Deng, S.; Jian, G.; Lei, J.; Hu, Z.; Ju, H. A Glucose Biosensor Based on Direct Electrochemistry of Glucose Oxidase Immobilized on Nitrogen-Doped Carbon Nanotubes. *Biosens. Bioelectron.* **2009**, *25* (2), 373−377.
(47) MacDougall, D.; Crummett, W. B.; et al. Guidelines for Data Acquisition and Data Quality Evaluation in Environmental Chemistry. *Anal. Chem.* **1980**, *52* (14), 2242−2249.
(48) Yun, Y. H.; Lee, B. K.; Choi, J. S.; Kim, S.; Yoo, B.; Kim, Y. S.; Park, K.; Cho, Y. W. A Glucose Sensor Fabricated by Piezoelectric Inkjet Printing of Conducting Polymers and Bienzymes. *Anal. Sci.* **2011**, *27* (4), 375−375.
(49) Bhat, K. S.; Ahmad, R.; Yoo, J.-Y.; Hahn, Y.-B. Nozzle-Jet Printed Flexible Field-Effect Transistor Biosensor for High Performance Glucose Detection. *J. Colloid Interface Sci.* **2017**, *506*, 188−196.
(50) Ma, J.; Jiang, Y.; Shen, L.; Ma, H.; Sun, T.; Lv, F.; Kiran, A.; Zhu, N. Wearable Biomolecule Smartsensors Based on One-step Fabricated Berlin Green Printed Arrays. *Biosens. Bioelectron.* **2019**, *144*, 111637.
(51) Abellán-Llobregat, A.; Jeerapan, I.; Bandodkar, A.; Vidal, L.; Canals, A.; Wang, J.; Morallón, E. A Stretchable and Screen-Printed Electrochemical Sensor for Glucose Determination in Human Perspiration. *Biosens. Bioelectron.* **2017**, *91*, 885−891.
(52) Chen, K.; Gao, W.; Emaminejad, S.; Kiriya, D.; Ota, H.; Nyein, H. Y. Y.; Takei, K.; Javey, A. Printed Carbon Nanotube Electronics and Sensor Systems. *Adv. Mater.* **2016**, *28* (22), 4397−4414.
(53) Li, L.; Pan, L.; Ma, Z.; Yan, K.; Cheng, W.; Shi, Y.; Yu, G. All Inkjet-Printed Amperometric Multiplexed Biosensors Based on Nanostructured Conductive Hydrogel Electrodes. *Nano Lett.* **2018**, *18* (6), 3322−3327.
(54) Ahmad, R.; Vaseem, M.; Tripathy, N.; Hahn, Y.-B. Wide Linear-Range Detecting Nonenzymatic Glucose Biosensor Based on CuO Nanoparticles Inkjet-Printed on Electrodes. *Anal. Chem.* **2013**, *85* (21), 10448−10454.
(55) Shamkhalichenar, H.; Choi, J.-W. An Inkjet-Printed Non-Enzymatic Hydrogen Peroxide Sensor on Paper. *J. Electrochem. Soc.* **2017**, *164* (5), B3101−B3106.
(56) Cinti, S.; Arduini, F. Graphene-Based Screen-Printed Electrochemical (bio)Sensors and Their Applications: Efforts and Criticisms. *Biosens. Bioelectron.* **2017**, *89*, 107−122.
(57) Cinti, S.; Arduini, F.; Moscone, D.; Palleschi, G.; Gonzalez-Macia, L.; Killard, A. J. Cholesterol Biosensor Based on Inkjet-Printed Prussian Blue Nanoparticle-Modified Screen-Printed Electrodes. *Sens. Actuators, B* **2015**, *221*, 187−190.
(58) Emaminejad, S.; Gao, W.; Wu, E.; Davies, Z. A.; Yin Yin Nyein, H.; Challa, S.; Ryan, S. P.; Fahad, H. M.; Chen, K.; Shahpar, Z.; Talebi, S.; Milla, C.; Javey, A.; Davis, R. W. Autonomous Sweat Extraction and Analysis Applied to Cystic Fibrosis and Glucose Monitoring Using a Fully Integrated Wearable Platform. *Proc. Natl. Acad. Sci. U. S. A.* **2017**, *114* (18), 4625−4630.

https://dx.doi.org/10.1021/acsami.0c02596
ACS Appl. Mater. Interfaces 2020, 12, 24231−24241